



# 1,3-Diphenyl-1*H*-pyrazole derivatives as a new series of potent PPAR $\gamma$ partial agonists

Jiwon Choi, Yunsun Park, Hui Sun Lee, Young Yang, Sukjoon Yoon \*

Sookmyung Women's University, Department of Biological Sciences, Hyochangwongil 52, Yongsan-gu, Seoul 140-742, Republic of Korea

## ARTICLE INFO

### Article history:

Received 20 August 2010

Revised 26 September 2010

Accepted 28 September 2010

Available online 26 October 2010

### Keywords:

Pyrazole

Peroxisome proliferators-activated receptor (PPAR)

Comparative molecular field analysis (CoMFA)

Computer-aided drug discovery

Molecular docking

Binding mode analysis

## ABSTRACT

A new series of PPAR $\gamma$  partial agonists, 1,3-diphenyl-1*H*-pyrazole derivatives, were identified using an improved virtual screening scheme combining ligand-centric and receptor-centric methods. An *in vitro* assay confirmed the nanomolar binding affinity of 1,3-diphenyl-1*H*-pyrazole derivatives such as SP3415. We also characterized the competitive antagonism of SP3415 against rosiglitazone at micromolar concentrations. They showed a PPAR $\gamma$  partial agonistic activity similar to that of a known PPAR $\gamma$  drug, pioglitazone, in a cell-based transactivation assay. Furthermore, the structure–activity relationships of the pyrazole derivatives were investigated through comparative molecular field analysis and binding mode analysis, which provided new insight concerning their partial agonistic effect on PPAR $\gamma$ .

© 2010 Elsevier Ltd. All rights reserved.

## 1. Introduction

The peroxisome proliferators-activated receptors (PPARs) comprise one of the most important subfamilies of nuclear receptor superfamilies, which functions as ligand-activated transcription factors regulating the expression of target genes.<sup>1</sup> To date, three subtypes of PPAR ( $\alpha$ ,  $\gamma$ , and  $\delta$ ) have been identified, and PPAR $\gamma$  is the most intensively studied subtype for drug discovery purposes. PPAR $\gamma$  is highly expressed in adipose tissue<sup>2</sup> and in blood cells and is induced during macrophage differentiation.<sup>3</sup> PPAR $\gamma$  was identified initially as a key regulator of adipogenesis, but it also plays an important role in type 2 diabetes, cellular differentiation, insulin sensitization, atherosclerosis, and cancer.<sup>4</sup> Rosiglitazone and pioglitazone are marketed PPAR $\gamma$  agonists that have been used in the treatment of type 2 diabetes.<sup>5</sup> However, it was recently suggested that rosiglitazone is associated with increased risk of cardiovascular events<sup>6</sup> and may cause adverse effects such as weight gain, fluid retention, and edema.<sup>7,8</sup> Judging from the several clinical studies, it is clear that rosiglitazone promotes a high risk for developing edema.<sup>9</sup> The adverse effects of PPAR $\gamma$  activators can be mitigated through use of partial PPAR $\gamma$  agonists, which can maintain the efficacy of full PPAR $\gamma$  agonists while lacking their typical side effects, such as edema and weight gain.<sup>10,11</sup> Therefore, it has been proposed that partial PPAR $\gamma$  agonists have improved safety margins

compared to full PPAR $\gamma$  agonists and might represent the next generation of insulin sensitizers. Recently, telmisartan,<sup>12–14</sup> metaglitazone,<sup>15</sup> balaglitazone,<sup>16,17</sup> and PA-082<sup>18</sup> were characterized as a new class of partial PPAR $\gamma$  agonists,<sup>19</sup> and several companies are trying to develop a novel PPAR $\gamma$  partial agonist that has potential effect without causing any increase in weight gain or edema.

The goal of the present study was to identify PPAR $\gamma$  partial agonists with novel scaffold and biological characteristics. Our previous study showed that ligand-centric and receptor-centric virtual screening methods are complementary to each other, and thus, a well-tuned combination of these methods can maximize virtual screening effectiveness.<sup>20</sup> An application of this advanced virtual screening procedure enabled us to efficiently identify ( $\beta$ -carboxyethyl)-rodanine derivatives as a novel series of PPAR $\gamma$  full agonists.<sup>21</sup> In this study, we combined the advantages of ligand-centric shape matching and receptor-centric docking methods to identify new PPAR $\gamma$  partial agonists with minimal experimental assays. As a result, we identified a new series of PPAR $\gamma$  partial agonists, 1,3-diphenyl-1*H*-pyrazole derivatives.

Pyrazole-based compounds have been widely explored as small molecular inhibitors of various targets such as p38 MAP kinase,<sup>22</sup> cathepsin S,<sup>23</sup> catechol-O-methyltransferase,<sup>24</sup> b-raf kinase,<sup>25</sup> co-activator associated arginine methyltransferase 1,<sup>26</sup> aurora kinase A,<sup>27</sup> and CDK.<sup>28</sup> It has been reported that pyrazole-based molecules have excellent drug-like properties and high oral bioavailability.<sup>29</sup> More recently, pyrazole-5-ylbenzenesulfonamide has been also reported as a PPAR partial agonist.<sup>30</sup> In the present

\* Corresponding author. Tel.: +82 2 710 9415; fax: +82 2 2077 7322.

E-mail address: [yoonsj@sookmyung.ac.kr](mailto:yoonsj@sookmyung.ac.kr) (S. Yoon).

study, we identified 1,3-diphenyl-1*H*-pyrazole derivatives as a series of PPAR $\gamma$  partial agonists and characterized their structure–activity relationship through comparative molecular field analysis (CoMFA). CoMFA is a widely used tool for 3D-QSAR studies.<sup>31–33</sup> CoMFA calculates steric and electrostatic properties according to Lennard-Jones and Coulomb potentials. Although several CoMFA studies have been performed on PPAR $\gamma$  agonists,<sup>34–38</sup> the SARs of pyrazole derivatives have not yet been investigated. We also characterized the binding mode of a pyrazole compound in the ligand-binding pocket of PPAR $\gamma$  in comparison with that of a known partial agonist. Our generated 3D-QSAR models and predicted binding mode provide useful insights into the influence of various interactive fields on the activity of the receptor and, thus, can help in designing improved partial PPAR $\gamma$  agonist molecules.

## 2. Results

### 2.1. Virtual screening of PPAR $\gamma$ partial agonists

Two different virtual screening strategies were employed to efficiently select a minimal set of potent PPAR $\gamma$  binders for the experimental assay. A ligand-centric 3D shape comparison method was used for the first step. Four known PPAR $\gamma$  partial agonists were used as the 3D queries for screening a chemical library (Fig. 1). A total of 1000 compounds with high 3D similarity to one of the query ligands were selected based on the ROCS combo score ( $\geq 0.95$ , see Methods for details). In the second step, structure-based virtual screening was carried out by using the shape-based distributed docking method which compromised the accuracy of multiple conformation docking and the speed of single conformation docking.<sup>20,30</sup> In our previous study, this method showed similar hit enrichment to multiple conformation docking by introducing a ligand-centric classification step, while it still maintained the speed of single conformation docking. Each of the selected compounds from the first step was assigned to the ligand class for which the compound showed the highest 3D shape similarity. Then, the compound was docked to the cognate PPAR $\gamma$  crystal

structure of the class-representing ligand. The chemical structures of four class-representing crystal ligands are displayed in Figure 1. As a result of this shape-based distributed docking, we selected a set of 100 compounds with the highest docking scores to PPAR $\gamma$ . Then, redundant compounds sharing similar 2D topologies (chemical structures) within the selected set were eliminated by using a Daylight descriptor (Tanimoto cutoff was 0.8). Finally, a total of 50 compounds were selected as the minimal set (Supplementary data) for use in an experimental FP assay that measured the direct binding affinity to PPAR $\gamma$ .

### 2.2. Biological assays of virtual hits

In the FP assay, the dissociation of the fluorescent PPAR $\gamma$  probe by competition with a test compound resulted in a low polarization value. Therefore, low FP signal indicates the high binding affinity of the compound with the PPAR $\gamma$  ligand binding domain (LBD). In the screening of 50 virtually selected compounds, we identified two compounds that showed significant affinity to PPAR $\gamma$  (Supplementary data). These two compounds have a common core structure, 1,3-diphenyl-1*H*-pyrazole, and were named as SP3300 and SP3400, respectively (Fig. 2A and B). The pyrazole structure also exists in a known PPAR $\gamma$  ligand, SP0 (3-fluoro-*N*-[1-(4-fluorophenyl)-3-(2-thienyl)-1*H*-pyrazol-5-yl]benzenesulfonamide) (Fig. 1). Consequently, it was noted that SP3300 and SP3400 had high 3D shape similarity to SP0 in the preceding virtual screening step. The overlay of SP3300 and SP3400 on SP0 shows a significant shape similarity (ROCS comboscores were 1.35 and 1.37, respectively), although their 2D chemical similarities to SP0 were not significant (Daylight Tanimotos were 0.35 and 0.29, respectively) (Fig. 2).

To investigate the structure–activity relationship of these compounds, we retrieved a total of 36 1,3-diphenyl-1*H*-pyrazole derivatives from commercial libraries and determined their binding affinity against PPAR $\gamma$  (Table 1). As a result, we found that seven compounds showed relatively high binding affinity to PPAR $\gamma$ , and thus, we further analysed their effect on PPAR $\gamma$  activation using a cell-based assay (Fig. 3). In comparison with well-known PPAR $\gamma$

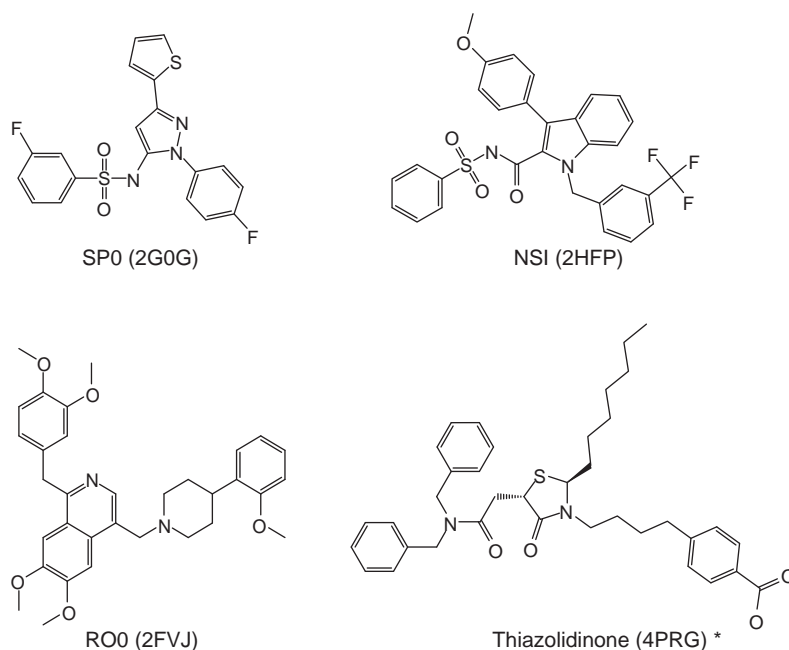


**Figure 1.** The structure of known PPAR $\gamma$  partial agonists used for the initial ligand-centric virtual screening. The 3D conformation of a ligand was taken from the crystal structure in complex with PPAR $\gamma$ . The PDB ID for each crystal structure is indicated in the bracket. \*The long aliphatic chain was removed before the shape comparison.

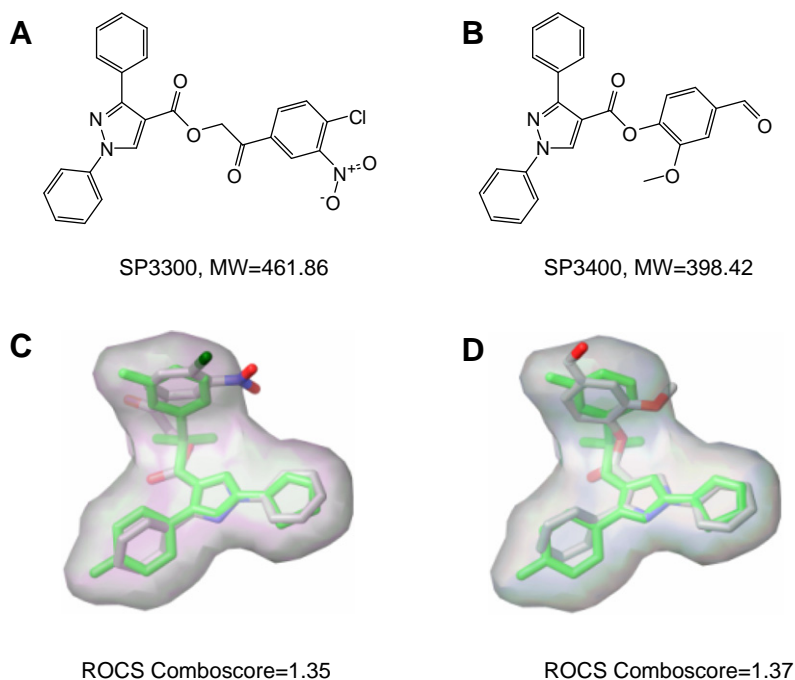


**Figure 2.** Two initial hits discovered by the virtual screening and consecutive in vitro binding assay. (A and B) The chemical structure of two hits named as SP3300 and SP3400, respectively. They have a common core structure, 1,3-diphenyl-1H-pyrazole. 3D shape similarity of identified hits to PDB ligand, SP0 is shown in (C) and (D). ROCS overlay of SP3300 and SP3400 (in green) was made on the crystal conformation of SP0 (in gray).

agonists, that is, rosiglitazone and pioglitazone, 1,3-diphenyl-1H-pyrazole derivatives showed relatively weak effects on the activation PPAR $\gamma$ . SP3415 induced the highest activation of PPAR $\gamma$  among the tested compounds. Initial hits, SP3300 and SP3400, did not show any significant effect on the activation of PPAR $\gamma$ , although they showed higher binding affinity to PPAR $\gamma$  than SP3415 and SP3416 in the in vitro binding assay.

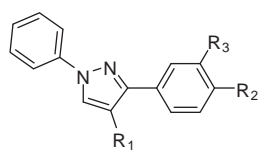
SP0, a selective partial agonist of human PPAR $\gamma$  (Fig. 1) is known to have a strong binding affinity to PPAR $\gamma$  ( $IC_{50}$  of 512 nM), but it had a relatively weak effect on the transactivation of PPAR $\gamma$  in comparison to rosiglitazone, a classic PPAR $\gamma$  full agonist.<sup>30</sup> Another PPAR $\gamma$  partial agonist, pioglitazone was shown to have over four-times weaker binding affinity to PPAR $\gamma$  than rosiglitazone (Fig. 4), which implies that high potency in terms of binding affinity does not necessarily represent high biological efficacy. SP3415 is similar to pioglitazone in terms of its levels of fold activation (Fig. 3) and binding affinity (Fig. 4). To confirm the partial agonism of SP3415 on PPAR $\gamma$ , we also carried out competitive activation assays between SP3415 and a strong agonist, rosiglitazone. Figure 5 shows in vitro transactivation of human PPAR $\gamma$  by SP3415 alone as well as by the combination of 1  $\mu$ M rosiglitazone with gradual increases in SP3415 concentration. This competition assay demonstrated that the increase of SP3415 concentration reduced the activation effect of rosiglitazone down to the level of SP3415 alone at the concentration of 10  $\mu$ M SP3415. Rosiglitazone was observed to be approximately five times more potent in terms of binding affinity to PPAR $\gamma$  than SP3415 (Fig. 4). Thus, the competitive antagonism of SP3415 against the effect of rosiglitazone at our given concentration confirms the partial agonism of SP3415 on PPAR $\gamma$ .

### 2.3. CoMFA and binding mode studies

To better understand the structure–activity relationship of SP3415 to PPAR $\gamma$ , CoMFA analysis was performed using all of the 36 1,3-diphenyl-1H-pyrazole derivatives. The docking pose of the most potent molecule, SP3415, was used as the alignment template, and the remaining molecules were superimposed to it. The analysis

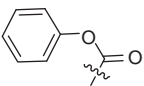
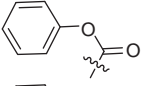
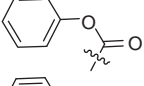
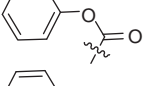
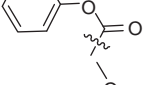
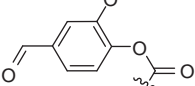
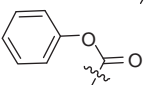
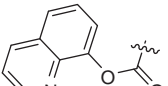
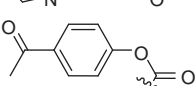
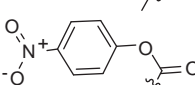
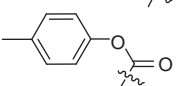
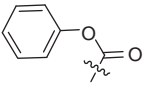
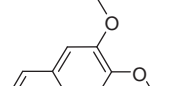
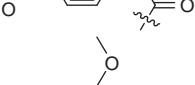
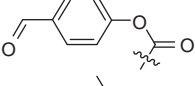
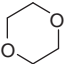
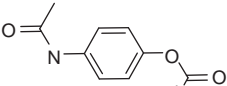
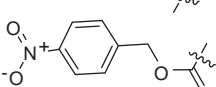
was performed by correlating variations in the binding affinity of the molecules with variations in their CoMFA fields using the partial least squares (PLS) method. Four molecules were removed as outliers that did not fit well into the CoMFA models. The statistical result of the best CoMFA model is summarized in Figure 6. The cross-validated  $q^2$ -value was 0.65, and the non-cross-validated  $r^2$  was 0.99 with six components. The statistical error in this model was reasonably low (the standard error estimate was 0.027). The conventional correlation coefficient represents the goodness of the fit of this model. The plot in Figure 6 shows the relationship between the predicted binding affinity and the experimental binding affinity values of the non-cross-validated analyses for the 32 1,3-diphenyl-1H-pyrazole compounds. Consistent with experimental data, SP3415 together with SP3300 and SP3400 showed higher binding affinities than other compounds in the CoMFA model.

The results of the CoMFA modeling are presented as contour maps that correlate the change in binding affinity with the molecular field values (Fig. 7A and B). Contour maps are useful in identifying possible interaction sites and important regions where any change in the steric or electrostatic field may affect the biological activity. From the PLS statistics in Figure 6, we found that the steric and electrostatic fields contributed almost equally to the CoMFA model. Sterically favored and disfavored regions (green and yellow in Fig. 7A) are scattered over the R1 and R2 regions. However, the favored green regions were only distributed in the R1 group, whereas the disfavored yellow regions were found in both R1 and R2 groups. The two big green contours observed in the R1 substitution indicate that any bulky group substitution at this position is favored for activity. This observation may be the reason why molecules with bulky substituents at this position, for example, SP3300, SP3400–3403, SP3405, SP3411, and SP3415, were more potent than compounds such as SP3408–3410 (Table 1). In the R2 and R3 regions, the presence of the two yellow contours suggests that bulky groups are disfavored for activity in this area. This model is consistent with the observation that compounds with no substituents in this area are generally more potent than those with any substituents. Figure 7B shows that the major electrostatic

**Table 1**The structure and binding affinity data of 1,3-diphenyl-1*H*-pyrazole derivatives against PPAR $\gamma$  LBD

Compound id	R1	R2	R3	Log (%binding)	CoMFA prediction
SP3300				1.98	1.99
SP3301		CH <sub>3</sub> O		1.42	1.42
SP3302		CH <sub>3</sub> O		1.57	1.29
SP3303		CH <sub>3</sub> O		1.20	1.45
SP3304		CH <sub>3</sub> O		1.05	1.65
SP3305				1.37	1.38
SP3306		Cl		1.15	1.15
SP3400				1.99	1.98
SP3401		Cl		1.81	1.47
SP3402		Br		1.73	1.75
SP3403		F		1.82	1.81
SP3404		CH <sub>3</sub> O	CH <sub>3</sub> O	1.64	1.66
SP3405		CH <sub>3</sub>		1.81	1.82

Table 1 (continued)

Compound id	R1	R2	R3	Log (%binding)	CoMFA prediction
SP3406		CH <sub>3</sub> O		1.45	1.50
SP3407				1.63	1.61
SP3408		CH <sub>3</sub>		1.31	1.60
SP3409		Cl		1.15	1.23
SP3410		Br		1.22	1.20
SP3411		CH <sub>3</sub> O	CH <sub>3</sub> O	1.82	1.81
SP3412		F		1.55	1.54
SP3413				1.52	1.48
SP3414				1.38	1.75
SP3415				1.90	1.91
SP3416		CH <sub>3</sub> O	CH <sub>3</sub> O	1.85	1.84
SP3417			NO <sub>2</sub>	1.38	1.38
SP3418		CH <sub>3</sub> O	NO <sub>2</sub>	1.36	1.38
SP3419		NO <sub>2</sub>		1.35	1.33
SP3420				1.50	1.50
SP4000				1.58	1.54
SP3800				1.38	1.37

(continued on next page)

Table 1 (continued)

Compound id	R1	R2	R3	Log (%binding)	CoMFA prediction
SP4700				1.72	1.73
SP2600				1.37	1.36
SP2800		F		1.68	1.67
SP3500		CH <sub>3</sub>		1.26	1.23
SP4500		F		1.63	1.63
SP4600				1.73	1.75

The FP-based binding affinity was measured at 10  $\mu$ M concentration of each compound. We converted the polarization values into logarithm unit binding affinity values.

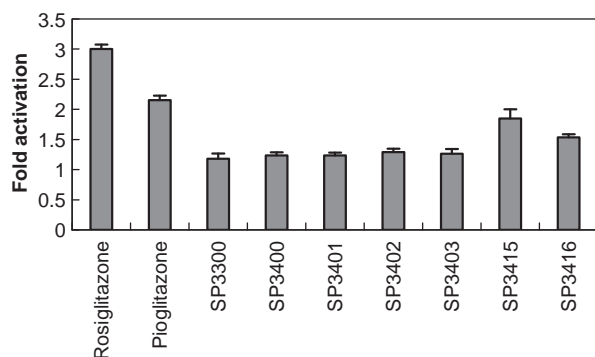


**Figure 3.** Activation of PPAR $\gamma$  by 1,3-diphenyl-1H-pyrazole derivatives. Compounds were treated on human embryonic kidney 293T cells with 10  $\mu$ M concentration, and the PPAR $\gamma$  activity was measured by luciferase reporter assay. For the positive control, 1  $\mu$ M rosiglitazone and pioglitazone were used.

interactions with the receptor also exist in the R1 region. The negative charge (red) was mainly distributed in the sterically favored green side of the R1 region, while the distribution of positive charge (blue) was not correlated to the steric fields. Thus, compounds SP3300, SP3400–3401, SP3405, and SP3414–15, which generally showed good binding affinities to the receptor, had bulky negative modifications in the favorable R1 position, whereas compounds SP3305, SP3413, SP3418, SP3420, SP3500, and SP3800, which showed relatively poor binding affinities, had positive or negative charges at the unfavorable position (Table 1). This model implies that further introduction of a negatively charged branches into the carbonyl group in R1 may be promising in terms of both steric and electrostatic interactions. We will synthesize various branched derivatives with increased negative charge in the future to further validate this QSAR model.

To better understand the activity of 1,3-diphenyl-1H-pyrazole derivatives at the molecular level, we carried out molecular docking of SP3415 at the PPAR $\gamma$  ligand-binding site. We used the crystal structures of PPAR $\gamma$  published as a complex with partial agonist

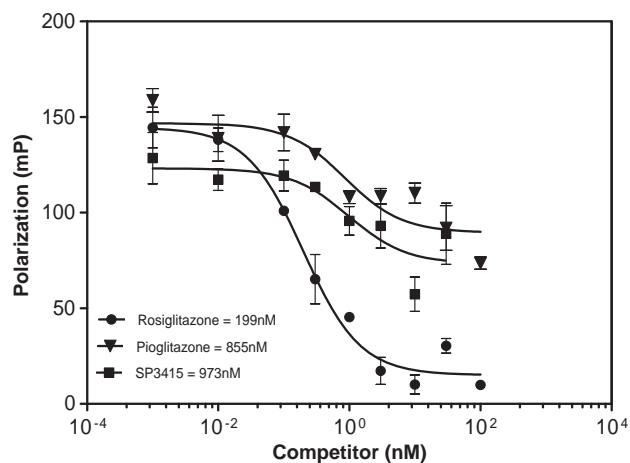


**Figure 4.** Relative affinity of SP3415, pioglitazone, and rosiglitazone to PPAR $\gamma$ -LBD. Error bar displays standard deviation from the mean of triplicate reactions in the assay. IC<sub>50</sub> of test compounds equal half-maximal shift in the polarization value.

ligand SP0 (PDB ID: 2G0G). For comparison, the crystal ligand SP0 was also re-docked, and the root mean-square deviation (RMSD) between the crystal pose and the docked pose was 0.21 Å. Figure 8A shows the similarity of the binding pose of SP3415 in comparison with the cognate crystal ligand, SP0. However, it was found that the –NO<sub>2</sub> substituent on the phenyl ring of SP3415 uniquely formed hydrogen-bond interactions with the side-chain NH of arginine 288 of PPAR $\gamma$  (Fig. 8B). This may provide the structural basis for the partial agonism of SP3415 many full agonists including rosiglitazone and pioglitazone have strong H-bonding interactions with Tyr473 in the binding pocket. In addition, the phenyl ring of SP3415, which corresponds to the sterically favorable R1 area in the CoMFA model, has strong hydrophobic interactions with the receptor, particularly with Ile341 and Tyr327 and also makes close contacts with Leu330. The spatial distribution of the backbone amino group of those three amino acids



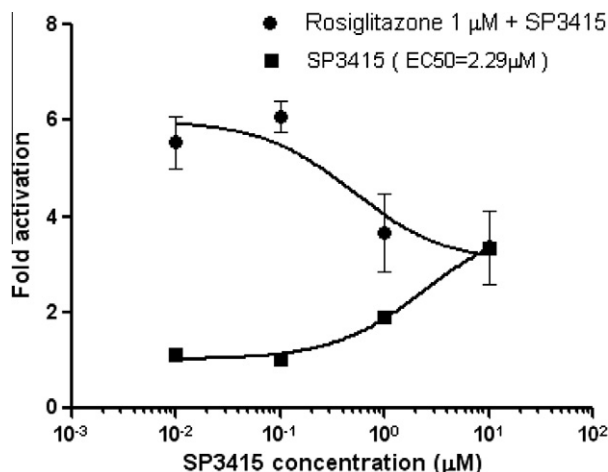


**Figure 5.** Dose–response curves on PPAR $\gamma$  for SP3415 alone and ‘SP3415 plus Rosiglitazone’. SP3415 retains weak agonist activity while it demonstrates competitive antagonism against rosiglitazone at  $\mu$ M concentrations.

implies that the further introduction of negatively charged groups at the interacting side of the SP3415 would increase the binding affinity between them. This charge distribution is consistent with the observations made from the CoMFA electrostatic contour map. Consistent with the cognate ligand SP0, SP3415 also forms pi-stacking interactions with the aliphatic side chains of L353,

F363, L356, and F360 that cover the hydrophobic ligand-binding pocket.

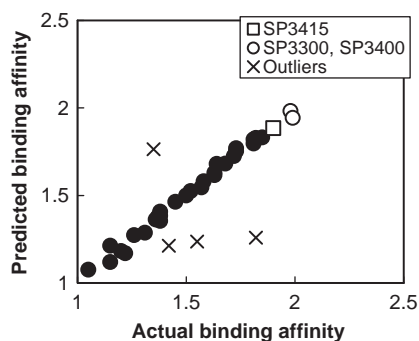
### 3. Conclusions

In this study, we identified novel partial PPAR $\gamma$  agonists, 1,3-diphenyl-1*H*-pyrazole derivatives, using an improved virtual screening method combining ligand-centric and receptor-centric methods. In the following experimental screening, two pyrazole-based compounds, SP3300 and SP3400, showed relatively strong binding activities against PPAR $\gamma$  among the virtual candidates. Upon further screening of 36 pyrazole derivatives, we found that SP3415 partially activated PPAR $\gamma$  with an IC<sub>50</sub> value of 973 nM, which was comparable to a known partial agonist, pioglitazone. In the competitive trans-activation assay with a full agonist, rosiglitazone, SP3415 showed antagonism against rosiglitazone at micromolar concentrations. Analysis of the CoMFA model and docking pose provided structural insights into the partial agonism of this compound and suggested a promising modification for further improvement of the agonist's binding affinity.

### 4. Methods

#### 4.1. Preparation of screening libraries

A collection of commercially available chemical libraries including approximately 300,000 non-redundant compounds in SDF format was used for the preparation of the virtual screening.



Statistical parameter	
$q^2$	0.65
No. of components	6
$r^2$	0.99
SEE	0.027
F value	465.1
Steric field contribution	0.46
Electrostatic field contribution	0.54

**Figure 6.** Scatter graph of the actual versus the predicted binding affinity of 1,3-diphenyl-1*H*-pyrazole derivatives by the best CoMFA model. A total of 32 molecules fit the model and four outliers were removed for the statistical analysis. The PLS statistics of CoMFA are summarized in the table.

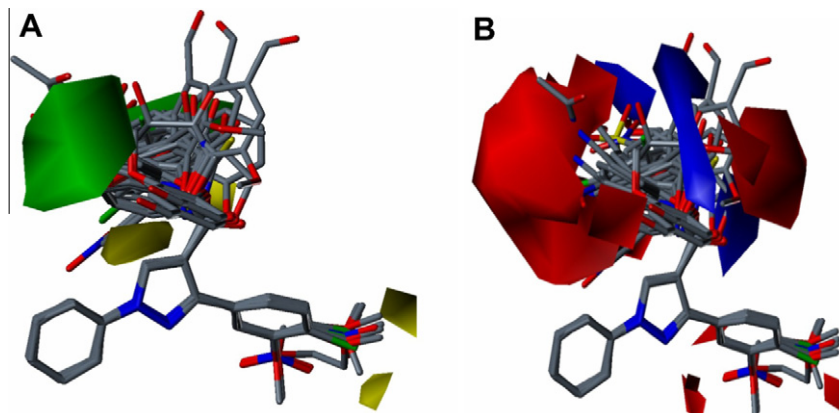


**Figure 7.** Alignment of pyrazole derivatives and contour maps for CoMFA model. The docked pose of SP3415 on PPAR $\gamma$  (PDB ID: 2G0G) was used as a template for the alignment. The aligned pyrazole derivatives, excluding outliers, were represented with a steric map (A) and an electrostatic map (B). The green color represents the sterically favored regions while the yellow represents the unfavored regions. Blue represents the electropositive group while red represents the electronegative group.

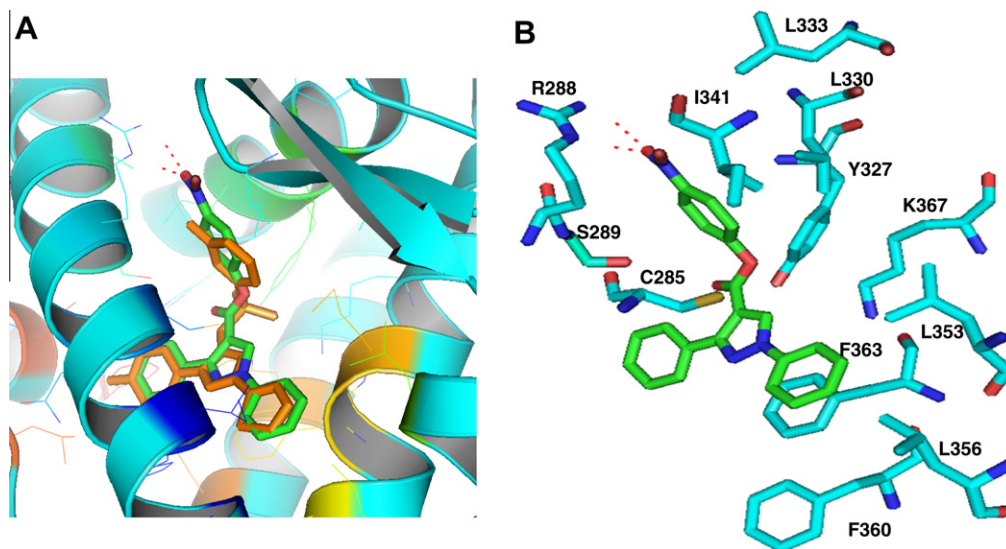


**Figure 8.** The binding pose of PPAR $\gamma$  ligand. (A) Comparison of SP3415 docking pose (green) with the binding mode of crystal ligand, SP0 (orange). (B) Major interaction of SP3415 with PPAR $\gamma$  binding pocket. Red dotted lines indicate hydrogen bonding interactions. The ligand is shown in green which forms hydrogen bonding interactions with NH group of Arg288 of PPAR $\gamma$ .

Compounds containing any atoms other than H, C, N, O, F, S, Cl, and Br were first removed using FILTER.<sup>39</sup> For ligand-centric shape comparison between PPAR $\gamma$  crystal ligands and library compounds, multiple conformers of each library compound were generated using the OMEGA program (version 2.1.0).<sup>40</sup> The maximum number of rotatable bonds was set to be large enough to accept all compounds. A maximum of 200 conformers were allowed for each compound based on a default RMSD cutoff (0.8 Å) and an energy window (25 kcal/mol).

#### 4.2. Ligand-centric virtual screening (shape comparison)

In the case of the crystal ligands, their crystal structures were used for the shape comparison without further conformation generation. Pairwise 3D shape similarities of the generated conformers against the crystal ligands were quantitatively calculated using the ROCS program (version 2.2).<sup>41</sup> ROCS (Rapid Overlay of Chemical Structures) is a program designed to perform large-scale structural comparisons through use of a superposition method. ROCS compares Gaussian-based overlaps parameterized to reproduce hard-sphere volumes between two molecules. As both the shape and electrostatic components of a molecule are critical for the observed biological activity, an overlap of functional groups was employed using properties such as hydrogen-bond donors and hydrophobic groups as well as shape-based matching. The degree of structural similarity between the two structures was calculated using the sum of the shape Tanimoto value and the scaled color value that ranged from 0 to 2, where 2.0 represents an exact match of both shape and functional groups between two molecules. To measure the chemical complementarity, we used the ImplicitMillsDean color force field, which is a simple  $pK_a$  model that defines cations, anions, donors, and acceptors.

#### 4.3. Receptor-centric virtual screening (molecular docking)

For molecular docking and scoring, PDB structures of PPAR $\gamma$  were prepared using the Schrödinger software package. All water molecules were removed and multimeric complexes were simplified from the PDB structure. If a PDB structure had missing side-chain atoms, Prime<sup>42</sup> was used to predict their location. Prior to the molecular docking, receptor structures were preprocessed

using protein preparation and refinement components from the Glide docking package.<sup>43</sup> Hydrogen atoms were added before the energy minimization. Side chains that were not close to the ligand-binding site and did not participate in salt bridges were neutralized. A restrained minimization using the OPLS-AA force field was performed for the refinement of the complex structure. This procedure reoriented side-chain hydroxyl groups and alleviated potential steric clashes. This minimization continued until the average RMS deviation of the non-hydrogen atoms reached the specified limit of 0.3 Å. The Glide docking algorithm performed a series of hierarchical searches for possible locations of the ligand in the binding site region of the receptor. The details of Glide docking and scoring methods are described elsewhere.<sup>44,45</sup> All compounds were energy-minimized using LigPrep and then docked to receptor structures using the standard mode of Glide docking (Glide SP 4.0).

To better understand the binding pose of SP3415, docking experiments were performed using the docking program GLIDE. The extra-precision (XP) modes of GLIDE were used for the accurate pose prediction.

#### 4.4. CoMFA modeling

Data set compounds were energy-minimized using standard Tripos force field after Gasteiger Huckel charges were assigned to all the structures. The alignment of dataset compounds is a critical factor in CoMFA modeling. Thus, we applied molecular alignment to align all the molecules used in the present study. The molecular alignment was achieved by a SYBYL (version 6.5, Tripos Inc.) routine database align. The most active compound (SP3415) was used as an alignment template, and the rest of the molecules were aligned to it using the common substructure. The aligned molecules are shown in Figure 7.

Steric and electrostatic interactions were calculated using the Tripos force field with a distance-dependent dielectric constant at all interactions in a regularly spaced (2 Å) grid using an  $sp^3$  carbon atom as the steric probe and a +1.0 charge as the electrostatic probe (the default probe atom in the SYBYL program). Steric and electrostatic fields were selected at 30.0 kcal/mol, which is the default energy cutoff value in SYBYL. With standard options for scaling of variables, the regression analysis was carried out using the fully



cross-validated partial least squares (PLS) method (leave one out). The optimal number of components used to derive the non-validated model was defined as the number of components leading to the highest cross-validated  $r^2$  and  $q^2$ .

#### 4.5. In vitro binding assay—fluorescence polarization (FP) assay

The PolarScreen™ PPAR Competitor Assay, Green kit (Invitrogen) was used for the evaluation of PPAR $\gamma$  binding activity of the virtually selected compounds. In this kit, the human PPAR $\gamma$  ligand-binding domain (PPAR-LBD) was tagged with an N-terminal His-tag and tight-binding, selective fluorescent PPAR $\gamma$  ligand, Fluormone PPAR Green. All test compounds was added into the wells of a 384-well microtiter plate and incubated with PPAR-LBD and Fluormone PPAR Green complex at room temperature for at least 2 h. The FP values were measured at the same concentration on a multi-detection microplate reader (SpectraMax M5 $^{\circ}$ ; Molecular Devices, Sunnyvale, CA) using 485-nm excitation and 535-nm emission interference filters. The maximum and minimum observable FP signals were used to obtain the %-fold activation value from the sample signal as follow,

$$\% \text{-fold activation} = 100 \times \frac{\text{max signal} - \text{sample signal}}{\text{max signal} - \text{min signal}}$$

Thus the possible range should be from 0% to 100%-fold change. When the log is applied to this, the range is from 0 to 2. The value of IC<sub>50</sub> was calculated by non-linear least squares curve fitting using GraphPad Prism 3.0 software (San Diego, CA, USA).

#### 4.6. Cell-based PPAR $\gamma$ activation assay—luciferase assay

The ligand binding domains (LBDs) of human PPARs (amino acids 167–468) and hPPAR $\gamma$  (amino acids 163–477) were generated by PCR amplification using Pfu polymerase and gene-specific primers flanked with restriction enzymes BamHI and XbaI. The LBDs were subcloned in frame into the pFA-CMV vector (Stratagene) to prepare pFA-Gal4-PPAR $\gamma$ -LBD. pFR-Luc and pRL-CMV plasmids were purchased from Stratagene and Promega, respectively. Human embryonic kidney 293T cells were plated in 12-well plates one day before the experiment, and transient transfection of the indicated genes was conducted using the calcium phosphate method. The next day, the cells were treated with test compounds and control compounds rosiglitazone and pioglitazone for a period of 24 h. The constitutively active pCMV-Renilla plasmid, which expresses *Renilla* luciferase, was used to normalize for transfection efficiency. The cells were washed twice with PBS and lysed in 300  $\mu$ l of reporter lysis buffer (Promega). The two luciferase activities were measured using a dual luciferase assay kit (Promega) on a microplate luminometer (Tuner Designs).

#### Acknowledgment

This research was supported by Sookmyung Women's University Research Grants 1-0803-0123.

#### Supplementary data

Supplementary data associated with this article can be found, in the online version, at doi:10.1016/j.bmc.2010.09.068.

#### References and notes

- Chawla, A.; Repa, J. J.; Evans, R. M.; Mangelsdorf, D. J. *Science* **2001**, 294, 1866.
- Braissant, O.; Foulfelle, F.; Scotto, C.; Dauca, M.; Wahli, W. *Endocrinology* **1996**, 137, 354.
- Ricote, M.; Li, A. C.; Willson, T. M.; Kelly, C. J.; Glass, C. K. *Nature* **1998**, 391, 79.
- Rosen, E. D.; Spiegelman, B. M. *J. Biol. Chem.* **2001**, 276, 37731.
- Sundriyal, S.; Bharatam, P. V. *Eur. J. Med. Chem.* **2008**, 44, 42.
- Nissen, S. E.; Wolski, K. N. *Engl. J. Med.* **2007**, 356, 2457.
- Gillies, P. S.; Dunn, C. J. *Drugs* **2000**, 60, 333.
- Hussein, Z.; Wentworth, J. M.; Nankervis, A. J.; Proietto, J.; Colman, P. G. *Med. J. Aust.* **2004**, 181, 536.
- Berlie, H. D.; Kalus, J. S.; Jaber, L. A. *Diab. Res. Clin. Pract.* **2007**, 76, 279.
- Berger, J. P.; Petro, A. E.; Macnaul, K. L.; Kelly, L. J.; Zhang, B. B.; Richards, K.; Elbrecht, A.; Johnson, B. A.; Zhou, G.; Doebber, T. W.; Biswas, C.; Parikh, M.; Sharma, N.; Tanen, M. R.; Thompson, G. M.; Ventre, J.; Adams, A. D.; Mosley, R.; Surwit, R. S.; Moller, D. E. *Mol. Endocrinol.* **2003**, 17, 662.
- Reifel-Miller, A.; Otto, K.; Hawkins, E.; Barr, R.; Bensch, W. R.; Bull, C.; Dana, S.; Klausner, K.; Martin, J. A.; Rafaloff-Phail, R.; Rafizadeh-Montrose, C.; Rhodes, G.; Robey, R.; Rojo, I.; Rungta, D.; Snyder, D.; Wilbur, K.; Zhang, T.; Zink, R.; Warshawsky, A.; Brozinick, J. T. *Mol. Endocrinol.* **2005**, 19, 1593.
- Benson, S. C.; Pershad Singh, H. A.; Ho, C. I.; Chittiboyina, A.; Desai, P.; Pravenec, M.; Qi, N.; Wang, J.; Avery, M. A.; Kurtz, T. W. *Hypertension* **2004**, 43, 993.
- Schupp, M.; Clemen, M.; Gineste, R.; Witt, H.; Janke, J.; Helleboid, S.; Hennuyer, N.; Ruiz, P.; Unger, T.; Staels, B.; Kintscher, U. *Diabetes* **2005**, 54, 3442.
- Kaschina, E.; Schrader, F.; Sommerfeld, M.; Kemnitz, U. R.; Grzesiak, A.; Krikov, M.; Unger, T. *J. Hypertens.* **2008**, 26, 2361.
- Allen, T.; Zhang, F.; Moodie, S. A.; Clemens, L. E.; Smith, A.; Gregoire, F.; Bell, A.; Muscat, G. E.; Gustafson, T. A. *Diabetes* **2006**, 55, 2523.
- Larsen, P. J.; Lykkegaard, K.; Larsen, L. K.; Fleckner, J.; Sauerberg, P.; Wassermann, K.; Wulff, E. M. *Eur. J. Pharmacol.* **2008**, 596, 173.
- Henriksen, K.; Byrjalsen, I.; Nielsen, R. H.; Madsen, A. N.; Larsen, L. K.; Christiansen, C.; Beck-Nielsen, H.; Karsdal, M. A. *Eur. J. Pharmacol.* **2009**, 616, 340.
- Burgermeister, E.; Schnoebelen, A.; Flament, A.; Benz, J.; Stihle, M.; Gsell, B.; Rufer, A.; Ruf, A.; Kuhn, B.; Marki, H. P.; Mizrahi, J.; Sebokova, E.; Nieser, E.; Meyer, M. *Mol. Endocrinol.* **2006**, 20, 809.
- Zhang, F.; Lavan, B. E.; Gregoire, F. M. *PPAR Res.* **2007**, 2007, 32696.
- Lee, H. S.; Choi, J.; Kufareva, I.; Abagyan, R.; Filikov, A.; Yang, Y.; Yoon, S. J. *Chem. Inf. Model.* **2008**, 48, 489.
- Choi, J.; Ko, Y.; Lee, H. S.; Park, Y. S.; Yang, Y.; Yoon, S. *Eur. J. Med. Chem.* **2010**, 45, 193.
- Walker, J. K.; Selness, S. R.; Devraj, R. V.; Hepperle, M. E.; Naing, W.; Shieh, H.; Kurambail, R.; Yang, S.; Flynn, D. L.; Benson, A. G.; Messing, D. M.; Dice, T.; Kim, T.; Lindmark, R. J.; Monahan, J. B.; Portanova, J. *Bioorg. Med. Chem. Lett.* **2010**, 20, 2634.
- Ameriks, M. K.; Bembek, S. D.; Burdett, M. T.; Choong, I. C.; Edwards, J. P.; Gebauer, D.; Gu, Y.; Karlsson, L.; Purkey, R. H.; Madsen, A. N.; Sun, S.; Thurmond, R. L.; Zhu, J. *Bioorg. Med. Chem. Lett.* **2010**, 20, 4060.
- Kiss, L. E.; Ferreira, H. S.; Torrao, L.; Bonifacio, M. J.; Palma, P. N.; Soares-da-Silva, P.; Lecomte, D. A. *J. Med. Chem.* **2010**, 53, 3396.
- Alzate-Morales, J. H.; Vergara-Jaque, A.; Caballero, J. J. *Chem. Inf. Model.* **2010**, 50, 1101.
- Huynh, T.; Chen, Z.; Pang, S.; Geng, J.; Bandiera, T.; Bindi, S.; Vianello, P.; Roletto, F.; Thieffine, S.; Galvani, A.; Vaccaro, W.; Poss, M. A.; Trainor, G. L.; Lorenzi, M. V.; Gottardis, M.; Jayaraman, L.; Purandare, A. V. *Bioorg. Med. Chem. Lett.* **2009**, 19, 2924.
- Coumar, M. S.; Leou, J. S.; Shukla, P.; Wu, J. S.; Dixit, A. K.; Lin, W. H.; Chang, C. Y.; Lien, T. W.; Tan, U. K.; Chen, C. H.; Hsu, J. T.; Chao, Y. S.; Wu, S. Y.; Hsieh, H. P. *J. Med. Chem.* **2009**, 52, 1050.
- Brasca, M. G.; Albanese, C.; Alzani, R.; Amici, R.; Avanzi, N.; Ballinari, D.; Bischoff, J.; Borghi, D.; Casale, E.; Croci, V.; Fiorentini, F.; Isacchi, A.; Mercurio, C.; Nesi, M.; Orsini, P.; Pastori, P.; Pesenti, E.; Pevarello, P.; Roussel, P.; Varasi, M.; Volpi, D.; Vulpatti, A.; Ciomei, M. *Bioorg. Med. Chem.* **2010**, 18, 1844.
- Goldstein, D. M.; Alfreidson, T.; Bertrand, J.; Browner, M. F.; Clifford, K.; Dalrymple, S. A.; Dunn, J.; Freire-Moar, J.; Harris, S.; Labadie, S. S.; La Fargue, J.; Lapiere, J. M.; Larrabee, S.; Li, F.; Papp, E.; McWeeney, D.; Ramesha, C.; Roberts, R.; Rotstein, D.; San Pablo, B.; Sjogren, E. B.; So, O. Y.; Talamas, F. X.; Tao, W.; Trejo, A.; Villaseñor, A.; Welch, M.; Welch, T.; Weller, P.; Whiteley, P. E.; Young, K.; Zipfel, S. J. *Med. Chem.* **2006**, 49, 1562.
- Lu, I. L.; Huang, C. F.; Peng, Y. H.; Lin, Y. T.; Hsieh, H. P.; Chen, C. T.; Lien, T. W.; Lee, H. J.; Mahindroo, N.; Prakash, E.; Yueh, A.; Chen, H. Y.; Goparaju, C. M.; Chen, X.; Liao, C. C.; Chao, Y. S.; Hsu, J. T.; Wu, S. Y. *J. Med. Chem.* **2006**, 49, 2703.
- Cramer, R. D., 3rd; Patterson, D. E.; Bunce, J. D. *Prog. Clin. Biol. Res.* **1989**, 291, 161.
- Waller, C. L.; Oprea, T. I.; Giolitti, A.; Marshall, G. R. *J. Med. Chem.* **1993**, 36, 4152.
- Carroll, F. I.; Gao, Y. G.; Rahman, M. A.; Abraham, P.; Parham, K.; Lewin, A. H.; Boja, J. W.; Kuhar, M. J. *J. Med. Chem.* **1991**, 34, 2719.
- Sundriyal, S.; Bharatam, P. V. *Eur. J. Med. Chem.* **2009**, 44, 42.
- Shah, P.; Mittal, A.; Bharatam, P. V. *Eur. J. Med. Chem.* **2008**, 43, 2784.
- Khanna, S.; Sobhia, M. E.; Bharatam, P. V. *J. Med. Chem.* **2005**, 48, 3015.
- Liao, C.; Xie, A.; Zhou, J.; Shi, L.; Li, Z.; Lu, X. P. *J. Mol. Model.* **2004**, 10, 165.
- Yi, X.; Guo, Z. R. *Yao Xue Xue Bao* **2001**, 36, 262.
- Filter, version 2.0.1; OpenEye Scientific Software, Inc.: Santa Fe, NM.
- Omega version 2.2.1; OpenEye Scientific Software, Inc.: Santa Fe, NM.
- Rocs version 2.3.1; OpenEye Scientific Software, Inc.: Santa Fe, NM.
- Prime, version 1.5; Schrödinger, LLC: Portland, OR.
- Glide, version 4.0; Schrödinger, LLC: Portland, OR.
- Friesner, R. A.; Banks, J. L.; Murphy, R. B.; Halgren, T. A.; Klicic, J. J.; Mainz, D. T.; Repasky, M. P.; Knoll, E. H.; Shelley, M.; Perry, J. K.; Shaw, D. E.; Francis, P.; Shenkin, P. S. *J. Med. Chem.* **2004**, 47, 1739.
- Friesner, R. A.; Murphy, R. B.; Repasky, M. P.; Frye, L. L.; Greenwood, J. R.; Halgren, T. A.; Sanschagrin, P. C.; Mainz, D. T. *J. Med. Chem.* **2006**, 49, 6177.